Available online at www.sciencedirect.com
ScienceDirect
International Journal of Solids and Structures 44 (2007) 6299–6317
INTERNATIONAL JOURNAL OF SOLIDS AND STRUCTURES
www.elsevier.com/locate/ijsolstr

The effect of non-uniformity of axial loading on the buckling behaviour of shells with random imperfections

Vissarion Papadopoulos *, Pavlos Iglesis

Institute of Structural Analysis and Seismic Research, National Technical University, Athens 15780, Greece

Received 6 October 2006; received in revised form 13 February 2007
Available online 20 February 2007

Abstract

In the present paper, the effect of random non-uniform axial loading on the buckling behaviour of isotropic thin-walled imperfect cylindrical shells is investigated. Random initial (out-of-plane) geometric imperfections, thickness and material property variability, together with a non-uniform stochastic axial loading are incorporated into a cost-effective non-linear stochastic finite element analysis using the non-linear TRIC shell element. For this purpose, the concept of an initial 'imperfect' structure is introduced involving not only deviations of the shell structure from its perfect geometry but also a spatial variability of the modulus of elasticity as well as of the thickness of the shell. The initial imperfections as well as the axial loading are modeled as stochastic fields with statistical properties that are either based on an available data bank of measured initial imperfections or assumed, in cases where no experimental data is available. Based on these simulation features, a simple and realistic approach is proposed for the estimation of the variability (scatter) of the limit loads by means of a brute-force Monte Carlo Simulation procedure. In addition, 'worst case' buckling scenarios are identified by means of a sensitivity analysis with respect to assumed parameters used for the description of stochastic fields that are not supported by corresponding experimental measurements. In addition it is shown that in the context of such sensitivity analysis, modeling of the non-uniformity of the axial loading is, from a computational point of view, fully equivalent to modeling the geometric boundary imperfections. The numerical tests performed demonstrate the significant role that the random varying axial loading plays on the buckling behaviour of imperfection sensitive structures like the axially compressed thin-walled cylinder considered in this study.

Keywords: Non-linear shell finite element, Non-uniform random axial loading; Random imperfections; Spectral representation; Evolutionary spectra

1. Introduction

The problem of buckling of imperfection sensitive shell-type structures has received a great deal of interest in the last decades. The major problem has always been the great discrepancy between theoretically predicted

* Corresponding author. Tel.: +30 210 7722625; fax: +30 210 7721693.
E-mail addresses: vpapado@central.ntua.gr (V. Papadopoulos), pauligle2000@yahoo.gr (P. Iglesis).

0020-7683/$ - see front matter © 2007 Elsevier Ltd. All rights reserved.
doi:10.1016/j.ijsolstr.2007.02.027

and experimentally observed buckling loads and also the wide scatter in the measured limit loads. It was soon realized, that the buckling behaviour of imperfection sensitive shells under axial loading is generally influenced by their initial geometric imperfections which produced during the manufacturing procedure. Early work on the subject mainly focused on the treatment of geometric imperfections using the Donnell-type theory together with Galerkin approximations of the solution that provided asymptotically accurate estimations at the bifurcation points (Koiter, 1963; Arbocz and Babcock, 1969; Hoff and Soong, 1969; Libai and Durban, 1977; Palassopoulos, 1977; Li, 1990; Greenberg and Stavsky, 1995; Li et al., 1997). Both deterministic and probabilistic approaches were implemented in the framework of the aforementioned analytic or semi-analytic methodologies. Probabilistic approaches were mainly implemented by treating the Fourier coefficients obtained by a series expansion of corresponding experimental measurements as random variables, while the simulation of the procedure was based on a Cholesky decomposition of the covariance matrix of the Fourier coefficients (Elishakoff, 1985; Elishakoff and Arbocz, 1985). Additional studies showed that geometric imperfections is not the only reason of the discrepancy between theory and experiments, and that the effect of thickness variability, material imperfections, imperfect boundary conditions as well as the non-uniformity of the applied axial load proved to be equally important leading to a further reduction of the predicted buckling loads (Arbocz and Babcock, 1969; Hoff and Soong, 1969; Libai and Durban, 1977; Greenberg and Stavsky, 1995; Li, 1990; Li et al., 1997; Elishakoff, 2000; Arbocz, 2000; Arbocz and Starnes, 2002; Elishakoff et al., 2001). As clearly stated in Schenk and Schueller (2003), the main disadvantage of these approaches was that they provided with limited capability in modeling more complex shell structures, while a realistic description of more general and combined imperfection patterns in a rational probabilistic context was elusive. As a result, the design process was -and still is- based on conservative corrections of the analysis via the well known empirical 'knock-down' factors.

Even though the reasons of the discrepancy and the scatter of the buckling loads were clearly understood and demonstrated at the 60's and 70's, it is only the last five to ten years that researchers focused on the combined effect of additional sources of imperfections together with the initial geometric ones. It is nowadays generally recognized that an accurate prediction of the buckling behaviour of shells requires a realistic description of all uncertainties involved in the problem and that such task is realizable only in the framework of a robust Stochastic Finite Element Method (SFEM) formulation that can efficiently and accurately handle the geometric as well as physical non-linearities of shell-type structures (Elishakoff, 2000; Arbocz, 2000; Arbocz and Starnes, 2002; Schenk and Schueller, 2003, 2005; Papadopoulos and Papadrakakis, 2004, 2005). Since the access to powerful computers became easier than ever, the analysis of such structures has been carried out in a probabilistic context through the application of the Finite Element method in conjunction with the Monte Carlo Simulation, incorporating realistic descriptions of the uncertainties involved in geometric (Schenk and Schueller, 2003) as well as material and thickness imperfections (Papadopoulos and Papadrakakis, 2004, 2005), which were modeled as stochastic fields using well established methodologies for their representation, e.g., Karhunen-Loeve expansion, Spectral Representation method and statistical properties that were either assumed, in cases where no experimental results were available, or based on experimental measurements (Arbocz and Abramovich, 1979). This type of SFEM approaches, however, can provide reasonable estimates of the scatter of the buckling loads only if the full probabilistic characteristics (marginal pdfs and correlation structures) of the involved stochastic fields are derived on the basis of corresponding experimental surveys. In cases where this is not possible, such approaches can only be implemented as 'worst case' studies, based on a sensitivity analysis with respect to the aforementioned parameters, leading this way to the assessment of the structural integrity of existing structures or to novel design procedures for new structures. A methodology for the achievement of an optimum design has recently been proposed in Lagaros and Papadopoulos (2006), where results of such sensitivity analysis were used in a reliability-based sizing-shape optimization of shell-type structures with random initial geometric material and thickness imperfections.

Non-uniformity of the axial loading as well as the uncertainty on the boundary conditions, were treated in the past using mainly the asymptotic theory without taking into account the combined effect of more than one sources of imperfections (Arbocz and Babcock, 1969; Hoff and Soong, 1969; Libai and Durban, 1977; Greenberg and Stavsky, 1995; Li, 1990; Arbocz, 2000). Despite the aforementioned disadvantages regarding the limitations of such methodologies, these early researches were pioneering in revealing the important role of these additional sources of imperfections on the buckling behaviour of shells. The approach used for modeling the

non-uniformity of axial loading was essentially equivalent to that of modeling the geometric boundary imperfections in the sense that both of them resulted in introducing a non-uniform axial load pattern acting on the cylinders' edges. This equivalence was made more evident in recent publications (Arbocz, 2000; Schenk and Schueller, 2005) where imperfections of the boundary conditions were modeled as in-plane geometric edge imperfections and were combined with the initial out-of-plane geometric imperfections in a non-linear finite element analysis using a two-step analysis procedure. As a first step, a prescribed displacement field was applied to the cylinders' edges, assuming full contact condition, and as a next step an incremental uniformly distributed displacement (Arbocz, 2000) or load (Schenk and Schueller, 2005) pattern was applied at the upper cylinders' edge. At this juncture it must be made clear that the use of the aforementioned approach is absolutely necessary in cases where experimentally measured edge imperfections have to be incorporated into the SFEM modeling. However, in the majority of cases such experimental results are not available. For example, only one relative experimental measurement of edge imperfections was found in Arbocz (2000) corresponding to an anisotropic cylinder. In such cases, the aforementioned two-step analysis procedure is not applicable and a sensitivity analysis has to be performed with respect to assumed parameters describing the probabilistic characteristics of edge imperfections.

In the present paper, a general, simple and realistic approach is proposed for modeling the geometric boundary imperfections in cases that experimental measurements are unavailable. As mentioned above, in such cases a sensitivity analysis with respect to assumed parameters describing the probabilistic characteristics of boundary imperfections, is necessary. The proposed methodology is based on the fact that in the context of a sensitivity analysis, the previously described two-step analysis procedure is fully equivalent to performing a sensitivity analysis with respect to the probabilistic characteristics of a random non-uniform axial load distribution applied as incremental load in the non-linear analysis. Thus, an edge deformation pattern is obtained at the very beginning of an incremental non-linear analysis procedure, which is assumed to correspond to the actual edge imperfections' pattern. A one-dimensional homogeneous stochastic field is used for modeling the applied axial load. This varying axial load together with the initial out-of-plane geometric imperfections, thickness and material properties variability are incorporated in a cost-effective non-linear SFEM analysis using the non-linear TRIC shell element (Argyris et al., 1997, 1998). The local average method is used for the derivation of the stochastic stiffness matrix (Argyris et al., 2002), while the variability of the limit loads is obtained by means of a brute-force Monte Carlo Simulation (MCS) procedure.

Furthermore, using the aforementioned approach, the present paper focuses on the study of the relative effect of a random non-uniform axial loading, or equivalently a random edge imperfection pattern, on the buckling load of isotropic thin-walled cylinders already possessing geometric out-of-plane, material and thickness imperfections. To the authors' knowledge, such investigation combining all the aforementioned sources of imperfections has not been presented so far. The numerical tests performed confirm the significant role of the non-uniform axial loading (or equivalently the random geometric boundary imperfections) on the buckling behaviour of imperfection sensitive structures like the thin-walled cylinder examined. In addition, the validity of the proposed methodology is enhanced by the reasonably close estimates obtained for the first and second order moments of the computed buckling loads, as well as of the shape of its probability distribution, with respect to experimental results. Finally, it must be mentioned that the proposed approach is general and can be applied for the numerical investigation of the buckling behaviour of any shell-type structure possessing boundary as well as geometric material and thickness imperfections.

2. Description of out-of-plane initial geometric imperfections

For the axially compressed cylinder of Fig. 2, out-of-plane initial geometric imperfections are modeled as a two-dimensional non-homogeneous stochastic field. The mean material and geometric properties of the perfect cylinder are also shown in Fig. 2. Following a procedure similar to the one used in Papadopoulos and Papadrakakis (2005), the mean values as well as the evolutionary power spectra of the aforementioned non-homogeneous fields are derived from corresponding experimental measurements (Arbocz and Abramovich, 1979).

The imperfect geometry of the shell is represented by the spatial variation of the radius of the structure as follows:

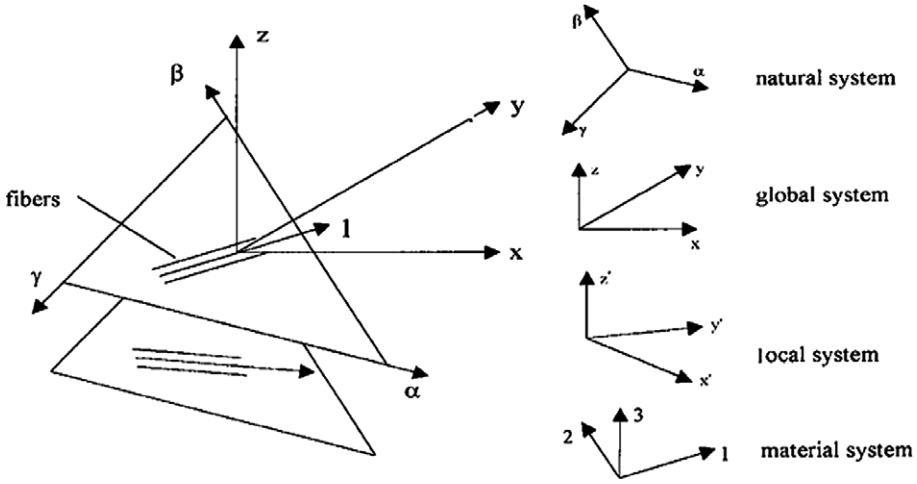

Fig. 1. The multilayer triangular TRIC element; coordinate systems.

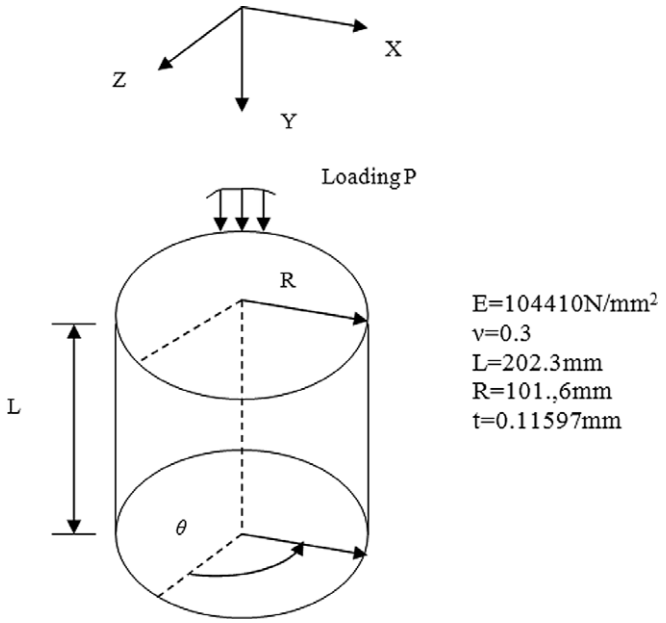

Fig. 2. Geometry and material data of the axially compressed cylinder.

$$r(x,y) = R + a_0(x,y) + f_1(x,y) \tag{1}$$

where $r(x,y)$ is the varying initial radius at each point of the structure, R is the radius of the perfect cylinder, $a_0(x,y)$ is the mean function of the imperfections with respect to the perfect geometry of the shell and $f_1(x,y)$ is a zero-mean non-homogeneous Gaussian stochastic field.

The mean function $a_0(x,y)$ as well as the properties of stochastic field $f_1(x,y)$ are derived from a statistical analysis of experimentally measured imperfections on seven copper electroplated cylindrical shells, named as A shells, depicted from a data bank of initial imperfections (Arbocz and Abramovich, 1979). The geometric and material properties of the corresponding perfect configurations of these shells as well as the corresponding experimental buckling loads are presented in Table 1. In Arbocz and Abramovich (1979) the measured initial imperfections are provided in the form of the following double Fourier series representation:

Table 1
Geometry, material properties and experimental buckling loads of A-shells (Arbocz and Abramovich, 1979)

Shell	R (mm)	t (mm)	L (mm)	E (N/mm^2)	P (N)
A-7	101.6	0.1140	203.20	104110	3036.4
A-8	101.6	0.1179	203.20	104800	3673.8
A-9	101.6	0.1153	203.20	101350	3724.8
A-10	101.6	0.1204	203.20	102730	3196.9
A-12	101.6	0.1204	209.55	104800	3853.0
A-13	101.6	0.1128	196.85	104110	3108.8
A-14	101.6	0.1110	196.85	108940	3442.9

$$w(x,y) = t \cdot \sum_{i}^{N} A_{i0} \cos\frac{i\pi x}{L} + t \cdot \sum_{k=0}^{N} \sum_{l=1}^{N} \cos\frac{\kappa\pi x}{L} \left(A_{kl} \cos\frac{ly}{R} + B_{kl} \sin\frac{ly}{R} \right) \tag{2}$$

where $w(x,y)$ is a function which extrapolates at each point x, y of the domain, the measured, in a grid of points, deviations from the unfolded cylinder's perfect geometry. In Eq. (2) A_{i0}, A_{kl} and B_{kl} denote the double Fourier series coefficients calculated for each wave number i, k and l, while L, R and t denote the length, the radius and the thickness of the perfect shell, respectively (see Fig. 2). A typical pattern of measured out-of-plane geometric imperfections $w(x,y)$, is plotted in Fig. 3 for the A7 shell specimen. As described in detail in Schenk and Schueller (2003) and Papadopoulos and Papadrakakis (2005), the interpretation of this pattern of imperfections as a sample function of the 2D stochastic field $w(x,y)$ of Eq. (2), indicates that $w(x,y)$ is clearly a non-homogeneous stochastic field with substantially varying first and second order properties.

The mean function $a_0(x,y)$ is calculated via ensemble averaging at each point of the unfolded cylinder as follows:

$$a_0(x,y) = \varepsilon[w(x,y)] \tag{3}$$

A plot of $a_0(x,y)$ is presented in Fig. 4. From this figure it can be observed that the mean value varies substantially along the two directions of the cylinder while, from the comparison of this figure with Fig. 3, it can be observed that the first order properties of the imperfections are mainly responsible for the amplitudes as well as for the basic pattern of the imperfections. It must be mentioned here that the value of the absolute maximum imperfection is selected as origin for the coordinate system in both the axial and the circumferential direction.

For the description of the non-homogeneous field $f_1(x)$ in Eq. (1), an evolutionary form of the spectral representation method is implemented (Papadopoulos and Papadrakakis, 2005; Lin et al., 2001; Shinozuka and Deodatis, 1996). The evolutionary power spectrum adopted in the present study is assumed to be uncoupled

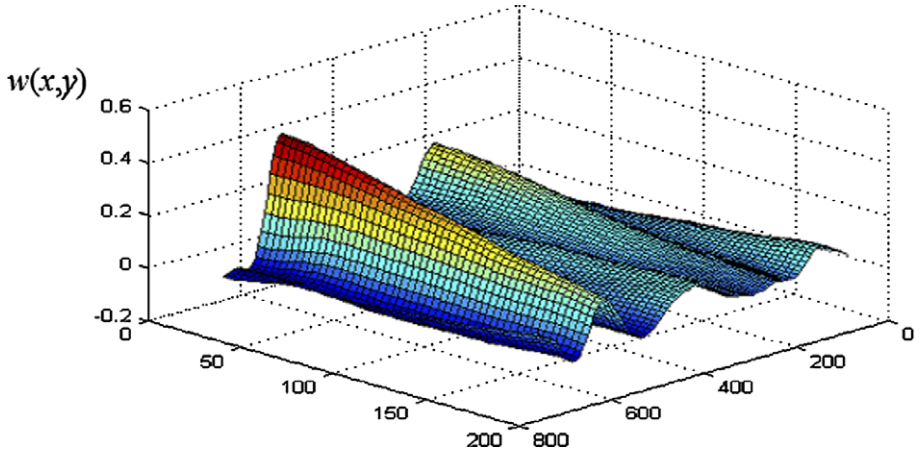

Fig. 3. Fourier series representation of measured initial unfolded shape of shell A7.

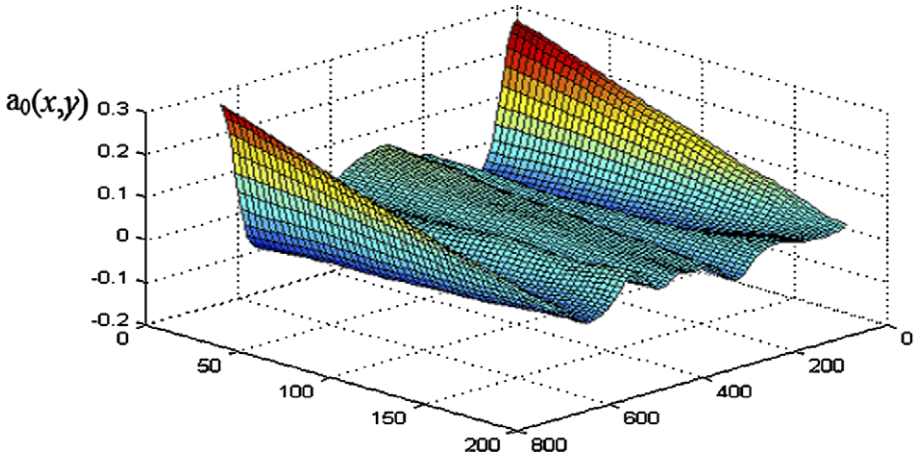

Fig. 4. Ensemble average of initial imperfections.

with respect to the axial and circumferential directions of the cylinder, since this is implied by the experimental measurements (refer to Fig. 3). Therefore, the evolutionary power spectrum used for the modeling of stochastic field $f_1(x)$ is written in the following form:

$$S^{\mathrm{E}}(\kappa_x, \kappa_y, x, y) = S_x^{\mathrm{E}}(\kappa_x, x) S_y^{\mathrm{E}}(\kappa_y, y) \tag{4}$$

where $S_x^{\mathrm{E}}(\kappa_x, x)$ and $S_y^{\mathrm{E}}(\kappa_y, y)$ are two independent one-dimensional power spectra for the axial and circumferential direction, respectively. These power spectra are obtained using a windows' sampling procedure, as follows:

$$S_x^{\mathrm{E}}(\kappa_x, x) = \frac{\int_{x-a}^{x+a} w(x, y=0) \exp[-2\pi \mathrm{i}(\kappa_x x)]\, \mathrm{d}x}{4\pi a} \tag{5a}$$

$$S_y^{\mathrm{E}}(\kappa_y, y) = \frac{\int_{y-b}^{y+b} w(x=0, y) \exp[-2\pi \mathrm{i}(\kappa_y y)]\, \mathrm{d}y}{4\pi b} \tag{5b}$$

The intervals $2a$ and $2b$ in Eqs. (5a) and (5b), respectively, define the dimensions of the moving window of the sample from which the power spectrum is estimated at each point of the discretized structure. Using Eqs. (5a) and (5b), the separate evolutionary 1D spectra are evaluated over each sample and averaged over the ensemble. The length of the sample used for the calculation of the spectrum at each grid point of the structure is selected to be $a = 0.01L$ and $b = 0.01\pi R$ for the axial and the circumferential direction, respectively. The

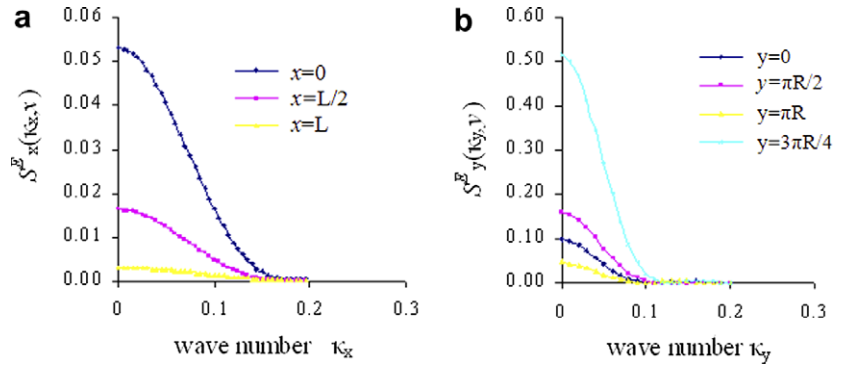

Fig. 5. Evolutionary power spectra of: (a) axial direction and (b) circumferential direction of the cylinder.

evolutionary power spectra along the directions of the cylinder are plotted in Fig. 5. From this figure it can be observed that the standard deviation varies substantially along the two directions of the cylinder, while the correlation length remains almost constant and equal to $b_x \approx 0.6L$ for the axial and $b_y \approx 0.06(2\pi R)$ for the circumferential direction. In addition, the evolutionary power spectrum seems to be uniformly modulated, since, as depicted in Fig. 5, the frequency content remains the same, while from the statistical analysis of the measured imperfections it occurs that the assumption of normality is in accordance with the experimental data.

3. Finite element simulation

The finite element simulation is performed using the TRIC non-linear triangular shell element, which is based on the natural mode method. The TRIC shear-deformable facet shell element is a reliable and cost-effective element suitable for linear and non-linear analysis of thin and moderately thick isotropic as well as composite plate and shell structures. The element has 18 degrees of freedom (6 per node) and hence 12 natural straining modes (Fig. 1). Three natural axial strains and natural transverse shear strains are measured parallel to the edges of the triangle. The stiffness is contributed by deformations only and not by the associated rigid-body motions. The natural stiffness matrix is derived from the statement of variation of the strain energy with respect to the natural coordinates.

The geometric stiffness is based on large deflections but small strains and consists of two parts. A simplified geometric stiffness matrix is generated by the rigid-body movements of the element and the natural geometric stiffness matrix due to the coupling between the axial forces and the symmetric bending modes (stiffening or softening effect). To construct the geometric stiffness, small rigid-body rotational increments about the local Cartesian axes are considered. These rigid-body rotational increments correspond to nodal Cartesian moments along the same axes. Only the middle plane axial natural forces are included in the stiffness matrix, which fully represent the prestress state within the material. In addition to the geometric stiffness corresponding to the rigid-body movements of the element, an approximate natural geometric stiffness arising from the coupling between the axial forces and the symmetric bending mode (stiffening or softening effect) is also considered. A full description of the linear elastic and geometric stiffness matrix of the TRIC shell element can be found in Argyris et al. (1997, 1998), respectively.

3.1. Stochastic stiffness matrix due to material and thickness imperfections

The modulus of elasticity and the thickness of the cylinder are considered to vary randomly in space. Therefore, these parameters are described by two independent 2D homogeneous stochastic fields as follows:

$$E(x,y) = E_0[1 + f_2(x,y)] \tag{6}$$

$$t(x,y) = t_0[1 + f_3(x,y)] \tag{7}$$

where E_0 is the mean value of the elastic modulus, t_0 is the mean thickness of the structure and $f_2(x,y)$, $f_3(x,y)$ are two zero-mean Gaussian homogeneous stochastic fields modeling the variability of the modulus of elasticity and the thickness of the shell, respectively. The two-sided power spectral density used to model stochastic fields $f_2(x,y)$, $f_3(x,y)$ is assumed to correspond to an autocorrelation function of exponential type and is given by:

$$S_{\mathrm{ff}}(\kappa_x,\kappa_x) = \frac{\sigma_{\mathrm{f}}^2}{4\pi} b_x b_y \exp\left[-\frac{1}{4}(b_x^2\kappa_x^2 + b_y^2\kappa_y^2)\right] \tag{8}$$

where σ_{f} denotes the standard deviation of the stochastic field and b_x, b_y denote the parameters that influence the shape of the spectrum, which are proportional to the correlation distances of the stochastic fields $f_2(x,y)$ and $f_3(x,y)$ along the x and y axes, respectively. The mean value and standard deviation of E and t are obtained from the corresponding experimental results presented in Table 1. The stochastic stiffness matrix of the TRIC shell element is derived using the local average method as described in detail in Argyris et al. (2002).

4. Non-uniformity of axial loading

Taking advantage of the, mentioned in Section 1, equivalence of modeling the non-uniformity of the axial loading and of modeling the geometric edge imperfections in the context of a sensitivity analysis, a simple and realistic approach is proposed for the treatment of edge imperfections by assuming that these are produced by a non-uniform random axial load distribution that can be modeled as a 1D homogeneous stochastic field assigning an equivalent concentrated force at each node of the discretized cylinder's edge, as follows:

$$P(x) = P_0[1 + f_4(x)] \tag{9}$$

where F_0 is the fixed (mean) value of the vertical applied load increment and $f_4(x)$ is a zero-mean Gaussian homogeneous stochastic field modeled with a two-sided power spectral density corresponding to an autocorrelation function of exponential type:

$$S_{\mathrm{ff}}(\kappa) = \frac{\sigma_{\mathrm{f}}^2}{4\pi} b_{\mathrm{f}} \exp\left[-\frac{1}{4}(b_{\mathrm{f}}^2\kappa^2)\right] \tag{10}$$

Thus, an edge deformation pattern is obtained at the very beginning of the incremental non-linear analysis procedure, which is assumed to correspond to the actual edge imperfections' pattern.

The validity of the aforementioned procedure for modeling the non-uniformity of the axial loading and the uncertainty on the boundary conditions, assuming that the two phenomena are essentially equivalent, can be further supported by the following: A flatness survey of one of the loading end rings used in a test setup of a stiffened axially compressed anisotropic cylinder was presented in Arbocz (2000). The results of this survey are depicted in Fig. 6, where a plot of the trace of the corresponding imperfections at the cylinder's edges is shown. Fig. 7 shows an ideal representation of the imperfect contact area of the cylinders' edge and its corresponding loading. It is clear that the edge is non-uniformly loaded, due to the in-plane geometric imperfections which do not allow a complete and solid contact between the cylinder and the loading member. As a result, the vertical load is applied as a series of point forces, non-uniformly distributed along the deformed edges of the cylinder.

Thus, using the proposed approach, the following effects are taken into account in the modeling: (i) non-uniformity of the end loads acting on both edges of the cylinder; (ii) contribution of the edge imperfections to the overall pre-buckling deformations; (iii) rotation of the end loading plates, usually observed in the experiments, which is indirectly represented with the overall bending moment introduced by the non-uniformity of

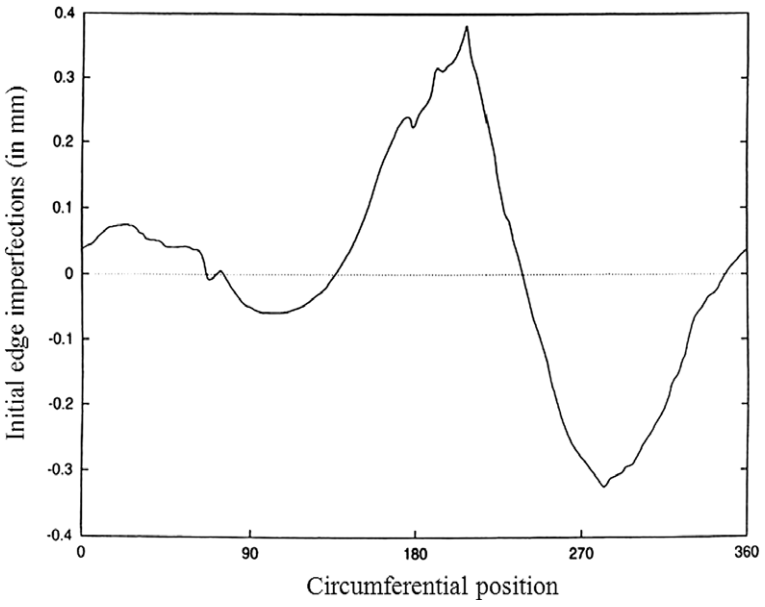

Fig. 6. Measured flatness of the end ring in Koiter (1963).

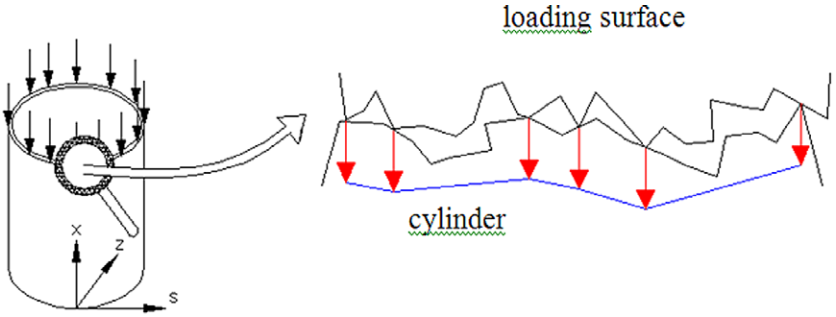

Fig. 7. Contact area of the cylinder and the loading surface.

the vertical loads and (iv) Vertical misalignment of the end loads which is directly related to the upper and lower out-of-plane edge imperfections. Finally, it must be mentioned that, despite the fact that stochastic $f_4(x)$ used for the modeling of the axial loading is assumed to be homogeneous, the resulting stochastic field of the edge displacements is clearly a non-homogeneous one, since this is obtained as a non-linear transformation of the homogeneous loading field.

5. Numerical results

The proposed methodology is implemented in the axially compressed cylinder of Fig. 2. The boundary conditions are specified as follows: the base edge nodes of the cylinder are fixed against all translations, fixed against rotations around the Y axis and free against rotations around the X and Z axis. The top edge nodes of the cylinder are fixed against X and Z translations, fixed against rotations around the Y axis, free against translations in the Y axis and free against rotations around axis X and Z.

For this problem, an extensive investigation was performed in Schenk and Schueller (2003), where imperfections were described as two-dimensional non-homogenous stochastic fields with statistical properties that were derived form a data bank of measured imperfections (Arbocz and Abramovich, 1979). An extension to this investigation that includes, not only the initial imperfect geometry but also the variability of the modulus of elasticity as well as the thickness of the cylinder, was recently presented in Papadopoulos and Papadrakakis (2005) where the concept of an initial 'imperfect' structure was adopted involving not only geometric deviations from its perfect geometry but also a spatial variability of the modulus of elasticity as well as of the thickness of the shell. In that work a sensitivity analysis was performed with respect to the standard deviation and correlation structure of the stochastic fields used for modeling these additional sources of imperfections since no experimental results were available. This sensitivity analysis focused on the effect of material and thickness imperfections on the buckling load of the imperfect cylinder with well defined (probabilistically) random geometric out-of-plane imperfections.

Mesh convergence studies were performed in Schenk and Schueller (2003) and Papadopoulos and Papadrakakis (2005) in order to determine an optimum FE mesh size satisfying the following two requirements: (i) Accurate prediction of the buckling load(s) of the cylinder and (ii) Accurate representation of the gradients of the stochastic initial imperfection field. The outcome of these studies was that refined meshes were required for an acceptable finite element prediction of the buckling load with respect to the 'exact' buckling load obtained with a semi-analytical procedure based on Donnell-type theory. In particular, a mesh of 101×191 was selected in Schenk and Schueller (2003) leading to a prediction of the normalized, with respect to the theoretical one, buckling load of $\lambda_{cr} = 0.8738$. The corresponding theoretical buckling load of the perfect cylinder is given by:

$$P_u^{(\text{perfect})} = \frac{Et^2}{R\sqrt{3(1-v^2)}} = 5350 \text{ N} \tag{11}$$

The numerically predicted critical buckling load corresponded to the load level at which the first negative eigenvalue of the tangent stiffness matrix of the structure appears, while the introduced discretization error

with respect to the 'exact' solution obtained with the semi-analytical method was of the order of 3% ($\lambda_{exact} = 0.8443$). The aforementioned 'exact' semi-analytic solution was obtained using the software tool ANALISA (Arbocz and Hol, 1991), which is based on Koiter's imperfection sensitivity theory (Koiter, 1963). Following a similar procedure, a mesh convergence study was performed in Papadopoulos and Papadrakakis (2005) using the same finite element approach with the one adopted in the present paper. The results of this convergence study are presented in Fig. 8. In this figure it can be seen that for a mesh of 51×401 the normalized buckling load was computed at $\lambda_{cr} = 0.857$ resulting in a relative, with respect to the 'exact' semi-analytic solution, error of the order of 1.5%.

The main disadvantage of the convergence studies performed in the aforementioned previous works was that these were performed with respect to the perfect cylinder's configuration, leading to possibly erroneous conclusions with respect to the buckling behaviour of the imperfect cylinder. In an effort to validate the proposed methodology, the same convergence study is repeated herein with respect to the imperfect cylinder and a randomly selected generation of geometric (out-of-plane) imperfections using Eq. (1). Fig. 9 presents the results of the convergence study of different mesh sizes. It can be observed that the coarse mesh of 51×101, produces a very small ($\sim$1%) relative discretization error of the buckling loads with respect to buckling loads calculated with more refined meshes. As shown in Fig. 8, the same error on the perfect cylinder is of the order of 15%. This dramatic reduction on the discretization error when the imperfect cylinder is considered instead of the perfect one can be explained by the fact that buckling modes of the imperfect cylinder are mainly characterized by the imperfections' pattern and not by some higher order modes of the perfect cylinder which require a very refined discretization in order to be captured by the FEM analysis. This observation leads to the important conclusion that relatively coarse meshes may be used for the buckling analysis of imperfect structures leading to cost-effective and accurate non-linear FEM simulations. Thus, the mesh of 51×101 was

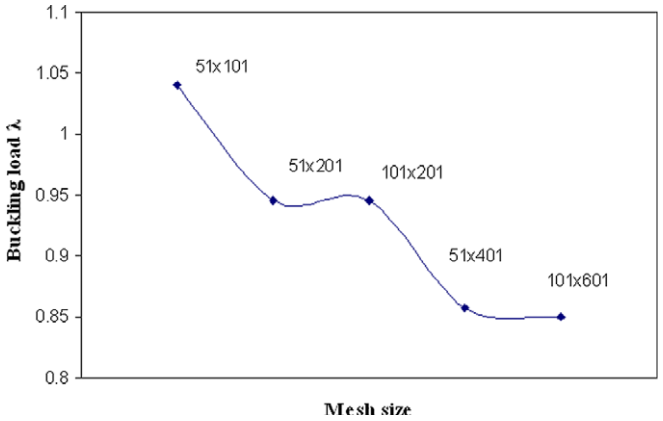

Fig. 8. Convergence behaviour of the perfect cylinder.

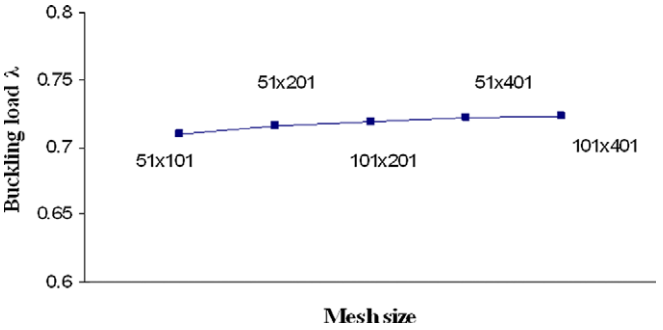

Fig. 9. Convergence behaviour of a randomly selected MC simulation of the imperfect cylinder loaded with a non-uniform axial load.

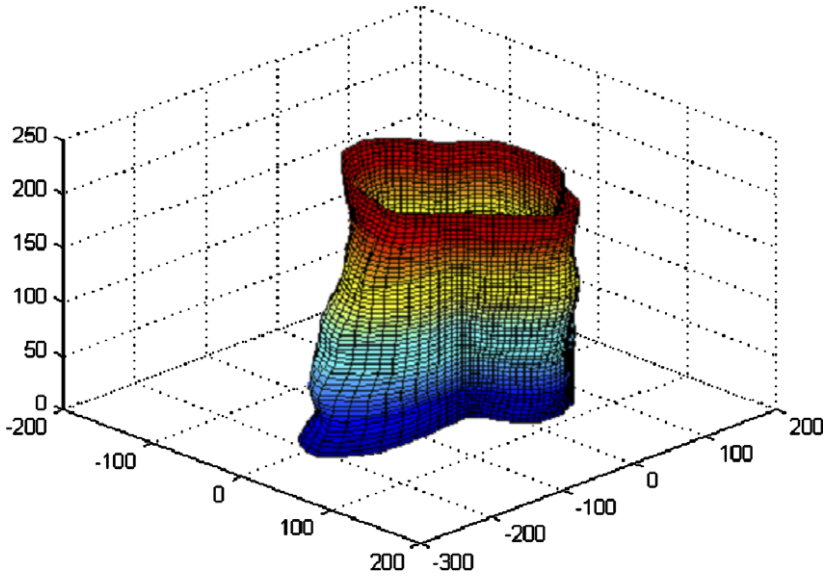

Fig. 10. Sample realization of non-homogeneous out-of-plane geometric imperfections using evolutionary power spectra theory and a mesh of 51×101.

adopted in the present study for subsequent applications and sensitivity studies. In addition, this mesh provides a sufficiently accurate representation of the gradients of the imperfect shape of the cylinder, since this mesh size is a fraction of the correlation lengths of the stochastic fields used for both axial and circumferential directions. This can be seen in Fig. 10 where a sample realization of initial geometric imperfections generated by Eq. (1) is presented for this particular mesh size.

5.1. Sensitivity analysis

5.1.1. Combination 1: non-uniformity of axial loading with out-of-plane geometric imperfections

A sensitivity analysis is performed with respect to the non-uniformity of the axial load on the cylinder already possessing initial geometric imperfections. This investigation, aiming at predicting 'worst case' scenarios, involves the generation of a family of different stochastic fields used for modeling the axial loading, which are introduced to the finite element model in addition to geometric out-of-plane imperfections. As will be demonstrated in the following paragraph, this family of stochastic fields corresponds to various initial edge deformation patterns. Samples of initial geometric out-of-plane imperfections are generated according to Eq. (1) using evolutionary spectra theory and a moving average model, based on a statistical analysis of experimentally measured initial imperfections (Arbocz and Abramovich, 1979). The family of stochastic fields used for modeling the axial loading is produced by the variation of the standard deviation σ_f and the correlation length parameter b_f of the power spectral density of Eq. (10) which is used for the description of stochastic field $f_4(x)$. For each set of selected σ_f and b_f parameters, a complete non-linear analysis (prediction of the buckling load) of the imperfect cylinder is performed.

Fig. 11 presents sample functions of the first load increment distribution $P(x)$ generated from Eq. (9), corresponding to four different values of the correlation length parameter ($b_f = 2$, $b_f = 10$, $b_f = 100$ and $b_f = 500$) and $\sigma_f = 0.1$. From this figure, it can be observed that the different spectral density functions used for the parametric study cover a wide range of possible scenarios for the stochastic field $P(x)$: From the almost random variable case ($b_f = 500$) to the almost white noise case ($b_f = 2$). Fig. 12 presents the edge deformation patterns which correspond to the previously described variations of the axial load distributions. From this figure it can be deduced that the displacement patterns obtained for $b_f = 2$, $b_f = 10$ and $b_f = 100$ have similar shapes, while the displacement pattern obtained for $b_f = 500$ is significantly different. It is particularly interesting to note the similarities between the shapes of the displacement patterns observed in Fig. 12 and those of Fig. 6 which are

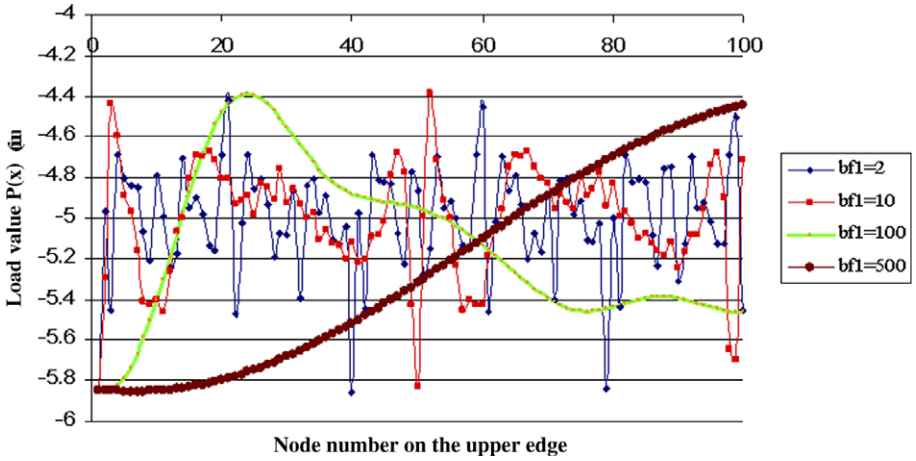

Fig. 11. First load increment distribution on the upper edge of the cylinder for different values of the correlation length parameter and $\sigma_f = 0.1$.

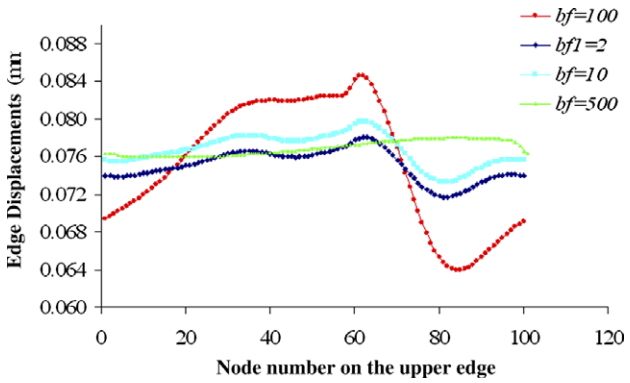

Fig. 12. Edge displacements of the upper edge of the cylinder for $\sigma_f = 0.2$.

experimentally measured edge imperfections as reported in Arbocz (2000). The similarities in shape between the measured and predicted edge imperfection patterns verify that the basic assumption adopted in this work, i.e that the initial edge imperfections can be reproduced by a non-uniform random load distribution on the upper edge of the cylinder, is realistic.

Figs. 13(a) and (b) present plots of the mean value and the coefficient of variation (COV) of the computed buckling loads respectively, as a function of the standard deviation σ_f, for various correlation length parameters ($b_f = 2$, $b_f = 10$, $b_f = 100$ and $b_f = 500$). From Fig. 13(a) it can be observed that the lowest mean buckling load for a standard deviation $\sigma_f = 0.3$ is obtained for a medium range of values of the correlation length parameters, reaching the value of $\overline{P}_u = 4068$ N and $\overline{P}_u = 4221$ N for $b_f = 10$ and $b_f = 100$, respectively. For this range of values, the results obtained for $b_f = 10$ and $b_f = 100$ are very similar. This similarity of buckling behaviour is also observed for the extreme range of values used for the correlation length parameters $b_f = 2$ and $b_f = 500$. In all cases, an almost linear reduction of the mean buckling load is observed as σ_f increases. These lower values of the mean buckling load predicted for the medium range of correlation length parameters can be explained by the shape of the typical load distributions for $b_f = 10$ and $b_f = 100$ shown in Fig. 11. As can be seen in this figure, a series of relatively large concentrated forces acting on half the circumference of the cylinder is accompanied by a series of relatively low values of concentrated forces, acting on the other half-circumference. This combination of relatively high and low nodal forces results in the maximization of the resulting overall moment acting on the upper edge of the cylinder leading to a significant reduction of the computed buckling loads. Similar conclusions can be derived from Fig. 13(b) with respect to the COV of

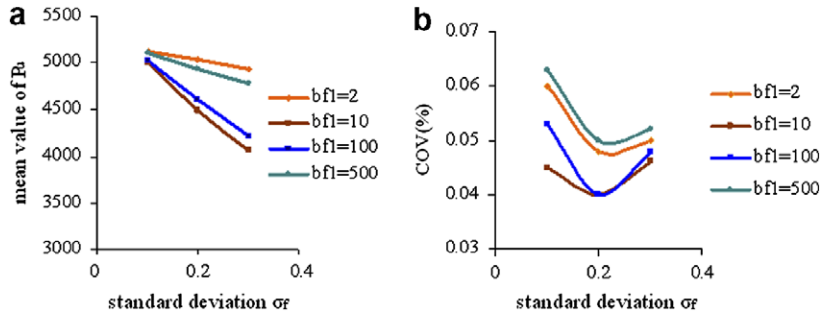

Fig. 13. Combination 1: (a) Mean value and (b) coefficient of variation of critical load factors plotted as a function of the standard deviation σ_f.

the computed buckling loads. For the medium range of correlation length parameters ($b_f = 10$ and $b_f = 100$) the COV appears to be always smaller compared to the COV obtained for the corresponding extreme values ($b_f = 2$ and $b_f = 500$), while a similarity of the COV behaviour is also observed with the medium or extreme values of correlation length parameters.

Figs. 14(a) and (b) present the histograms of the buckling loads for the aforementioned selected values $b_f = 10$ and $b_f = 100$, respectively and standard deviation $\sigma_f = 0.1$. For reasons of comparison, the loads are normalized with respect to the predicted buckling load of the perfect cylinder using the mesh of 51×101 ($P_u^{(\text{perfect})} = 5350$ N). The mean value and the coefficient of variation of the predicted buckling loads are found to be $\overline{P_u} = 5004$ N and $\overline{P_u} = 5022$ N, while the coefficient of variation was calculated at COV = 0.041148 and COV = 0.055542, respectively. From these figures it can be observed that the predicted mean values for the two correlation lengths almost coincide, while for $b_f = 100$ a 25% larger value for the COV was calculated. Figs. 15(a) and (b) and 16(a) and (b) present similar plots for standard deviations $\sigma_f = 0.2$ and $\sigma_f = 0.3$, respectively. For $\sigma_f = 0.2$, the mean value of the predicted buckling loads is found to be $\overline{P_u} = 4496$ N

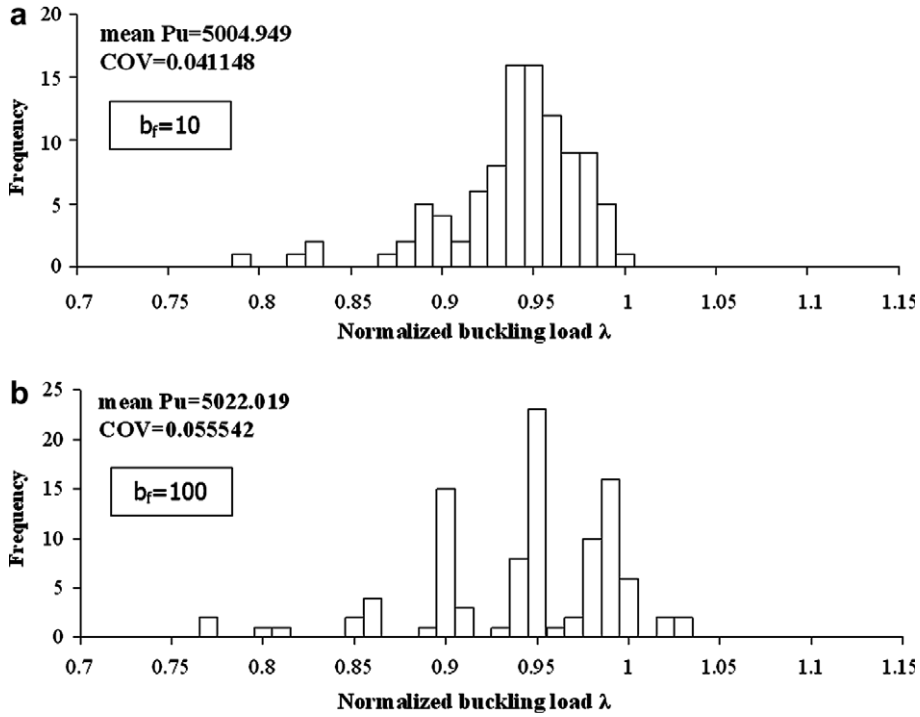

Fig. 14. Combination 1: Histograms of critical load factors for (a) $b_f = 10$, (b) $b_f = 100$ and $\sigma_f = 0.1$.

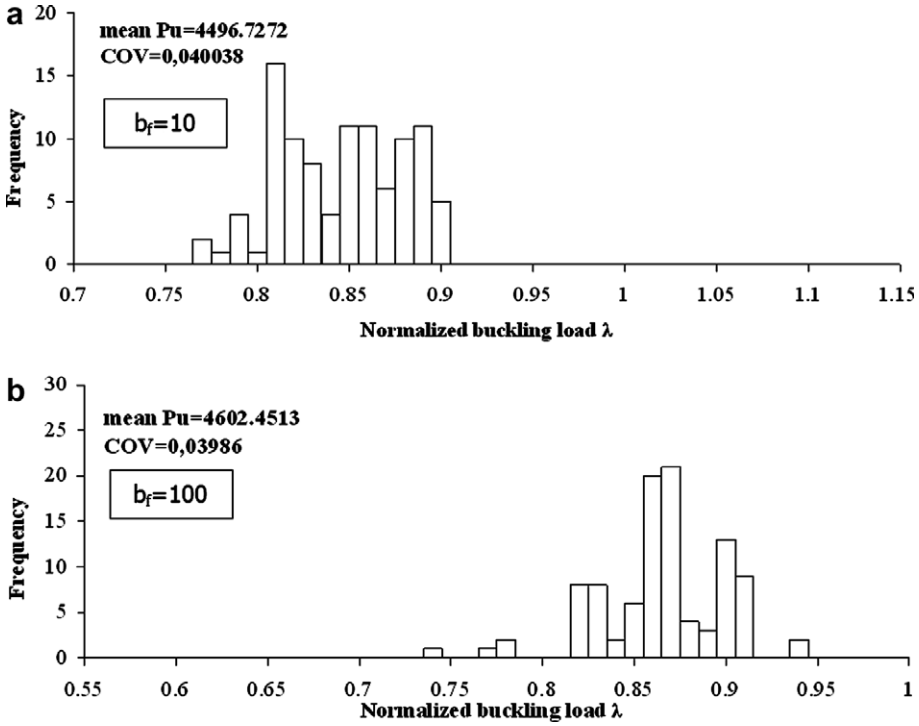

Fig. 15. Combination 1: Histograms of critical load factors for (a) $b_f = 10$, (b) $b_f = 100$ and $\sigma_f = 0.2$.

and $\overline{P_u} = 4602$ N, for $b_f = 10$ and $b_f = 100$, while the coefficient of variation is calculated at COV = 0.040038 and COV = 0.03986, respectively. The corresponding to $\sigma_f = 0.3$ computed values are found to be $\overline{P_u} = 4068$ N, $\overline{P_u} = 4221$ N and COV = 0.04611, COV = 0.04807 for $b_f = 10$ and $b_f = 100$, respectively. From these figures, it can be observed that the buckling behaviour of the cylinder for $\sigma_f = 0.2$ and $\sigma_f = 0.3$ is almost the same for the two selected correlation length parameters, while from the comparison of these figures with Figs. 14(a) and (b) a reduction of the predicted mean values can be observed. This reduction can be attributed to the increase of the standard deviation σ_f leading to larger amplitudes of the initial in-plane edge imperfections.

Fig. 17 presents the histogram of the computed in Papadopoulos and Papadrakakis (2005) buckling loads, where initial out-of-plane geometric imperfections were assumed as a stand alone case. In the aforementioned calculation, the mean value and the coefficient of variation of the predicted buckling loads were found to be $\overline{P_u} = 4800$ N and COV = 0.07548, respectively. From the comparison of Figs. 14–16 with Fig. 17, it can be seen that the incorporation of the imperfections on the boundary conditions into the model of initial geometric imperfections resulted in a decrease up to 25% in the coefficient of variation, for all levels of the standard deviation considered, while a reduction of the predicted mean value is observed for $\sigma_f = 0.2$ and $\sigma_f = 0.3$, reaching the order of 15% for the largest standard deviation ($\sigma_f = 0.3$). Thus, it can be generally concluded that only medium range correlation length parameters have a significant effect on the buckling behaviour of the imperfect cylinder. This effect corresponds to a substantial reduction on the mean value of the buckling loads followed by a decrease of the COV with respect to the imperfect cylinder loaded with a uniformly applied axial load. This can be explained by the fact that the two extreme cases of $b_f = 2$ and $b_f = 500$ are close to the white noise and the random value case, respectively, which resemble the case of a uniformly applied axial load. Therefore, the medium range values of $b_f = 10$ and $b_f = 100$ is selected for all subsequent applications since for these values, 'worst case' scenarios are more likely to occur with respect to the lowest values of the predicted buckling loads.

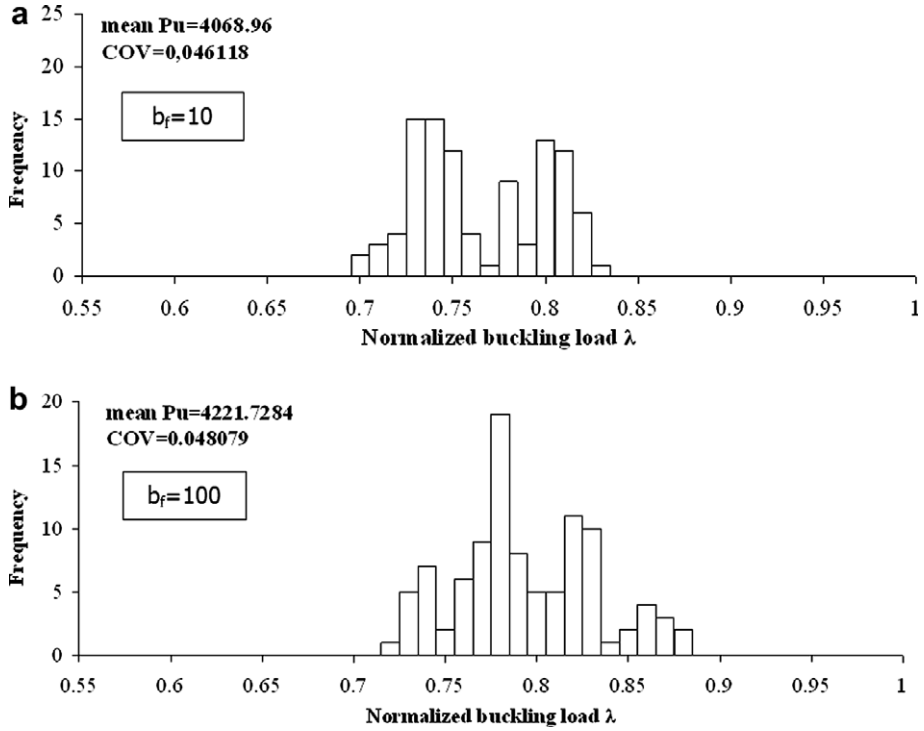

Fig. 16. Combination 1: Histograms of critical load factors for (a) $b_f = 10$, (b) $b_f = 100$ and $\sigma_f = 0.3$.

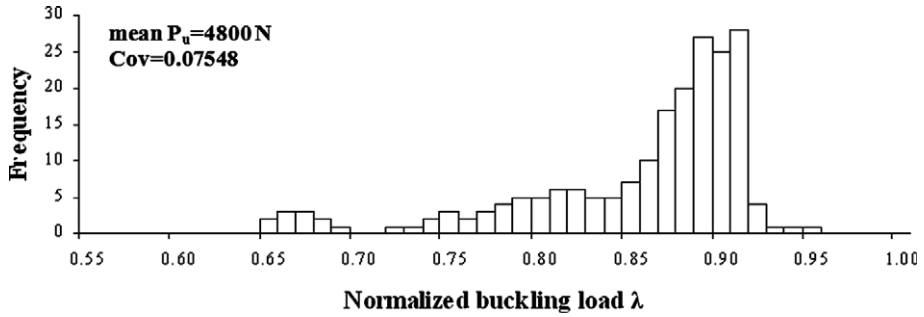

Fig. 17. Histograms of critical load factors obtained in Elishakoff et al., 2001 for initial out-of-plane geometric imperfections.

5.1.2. Combination 2: geometric out-of-plane imperfections with material and thickness imperfections

A sensitivity analysis was performed in Papadopoulos and Papadrakakis (2005) in order to investigate the effect of material and thickness variability on the buckling behaviour of the uniformly compressed cylinder with initial out-of-plane geometric imperfections. The basic results of the aforementioned investigation are repeated here for reasons of completeness. The sensitivity analysis was performed with respect to the correlation length parameters of the stochastic fields used for the description of material and thickness variability, since, as in the case of the non-uniformity of the axial loading, no experimental data is available for the variability of these additional imperfection parameters. The standard deviation of modulus of elasticity and thickness are derived from the experimental measurements in Arbocz and Abramovich (1979) (see Table 1) and found to be 10% and 1%, respectively, while it is assumed that the correlation length parameters are equal in both directions. As described in Section 3.1, the stochastic fields used for the modeling of the aforementioned material properties were assumed to be Gaussian. This Gaussian assumption, although physically wrong for material properties that cannot assume negative values, is adopted here for reasons of simplicity

and as a first step to our investigation. However, it is guaranteed that a negative value of a material property cannot practically occur for the relatively small values depicted for the standard deviations of these parameters (10% and 1% for the modulus of elasticity and thickness, respectively). The effect of other non-Gaussian fields modeling these parameters on the buckling behaviour of shells is a subject of future research.

As a first step, the variability of modulus of elasticity and thickness were considered as stand alone cases. Figs. 18(a) and (b) present the mean value and coefficient of variation of the ultimate load P_u of the perfect cylinder as a function of the correlation length parameters $b_1 = b_2$ for variability of modulus of elasticity and thickness, respectively. From Fig. 18(a) it can be seen that for the case of the modulus of elasticity the lowest mean buckling load reaches the value of $\overline{P_u} = 4387$ N and is obtained for $b_1 = b_2 = 50$ mm, while the COV remains almost constant and equal to COV = 0.1. From Fig. 18(b) it can also be observed that for the case of thickness variability the mean value of the predicted buckling loads remains constant and equal to $\overline{P_u} = 5085$ N, while the coefficient of variation varies from 10% to 20% for $b_1 = b_2 = 50$ mm and $b_1 = b_2 = 500$ mm, respectively. Fig. 17 demonstrates the important role of these sources of imperfections

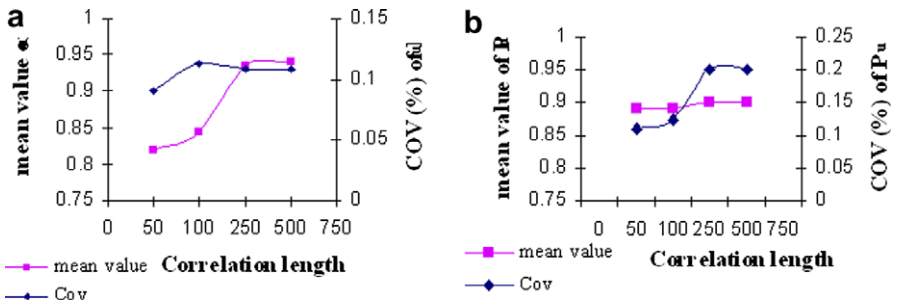

Fig. 18. Mean value and coefficient of variation (COV) of the ultimate load P_u of the perfect cylinder as a function of the correlation length parameters $b_1 = b_2$, for: (a) 2D variation of the modulus of elasticity and (b) 2D variation of the thickness.

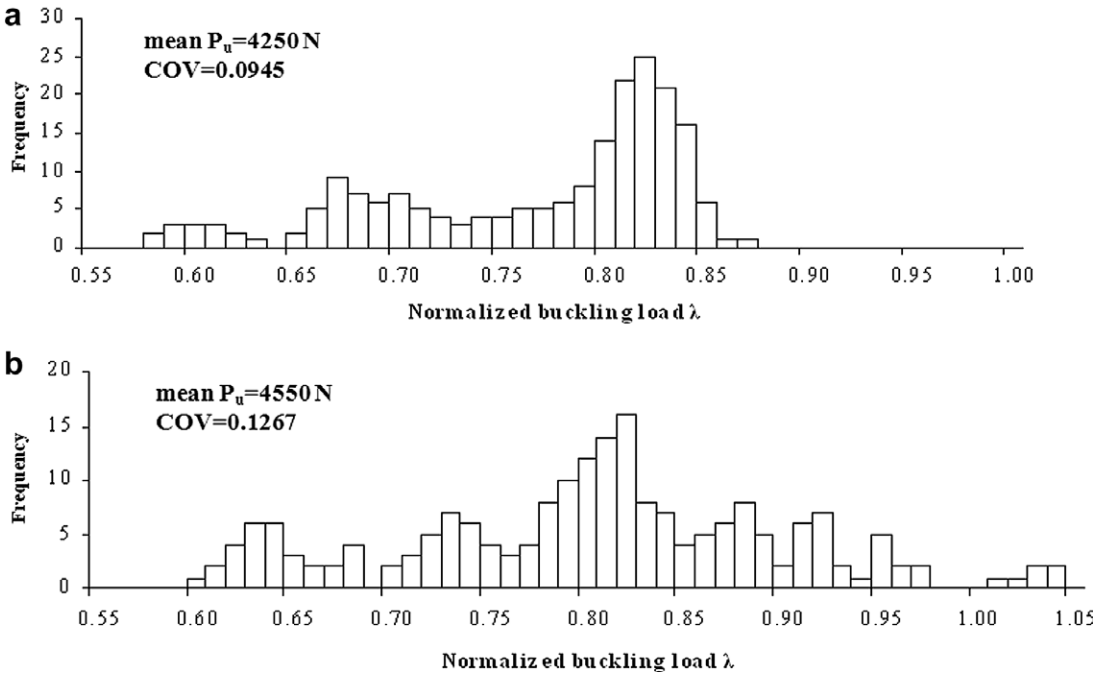

Fig. 19. Combination 2: Histograms of critical load factors for correlation length parameters of the modulus elasticity and thickness (a) $b_1 = b_2 = 50$ mm and (b) $b_1 = b_2 = 500$ mm.

on the buckling behaviour of the cylinder even if they are considered as stand alone cases. Therefore the values of $b_1 = b_2 = 50$ mm and $b_1 = b_2 = 500$ mm for the correlation length parameters, respectively, were selected for both modulus of elasticity and thickness, since these values are responsible for the minimum mean and the maximum variance of the buckling loads of the perfect cylinder when material and thickness imperfections are considered as stand alone cases.

Material and thickness imperfections were then combined and introduced simultaneously to the model of the imperfect cylinder. Figs. 19(a) and (b) present the histograms of the buckling loads of the cylinder for correlation lengths of modulus of elasticity and thickness $b_1 = b_2 = 50$ mm and $b_1 = b_2 = 500$ mm, respectively. The mean value of the predicted buckling loads is found to be $\overline{P_u} = 4250$ N and $\overline{P_u} = 4550$ N, while the coefficient of variation is found to be 0.0945 and 0.1267 for $b_1 = b_2 = 50$ mm and $b_1 = b_2 = 500$ mm, respectively. Therefore the values of $b_1 = b_2 = 50$ were selected for all subsequent applications since for these values it is are more likely to occur 'worst case' scenarios with respect to lowest buckling loads.

5.1.3. Combination 3: non-uniformity of the applied axial load with out-of-plane geometric, material and thickness imperfections

Last step of the present study is to introduce simultaneously into the model the material and thickness sources of imperfections and the initial out-of-plane geometric imperfections and imperfections of the boundary conditions. Based on the results presented in previous sections, the correlation length parameter $b_f = 100$ with $\sigma_f = 0.2$ and $\sigma_f = 0.3$ is selected for the description of the stochastic field $f_4(x)$ used to model the load distribution on the upper edge of the cylinder. For the description of the modulus of elasticity and thickness the correlation length parameters $b_1 = b_2 = 50$ were selected. Figs. 20(a) and (b) present the histograms of the buckling loads for the analysis of this last combination for a standard deviation of the axial loading $\sigma_f = 0.2$ and $\sigma_f = 0.3$, respectively. From Fig. 20(a) it can be observed that for $\sigma_f = 0.2$ the mean value of the predicted buckling loads is found to be $\overline{P_u} = 3833$ N, the coefficient of variation is found to be COV = 0.08728 and the lowest buckling load was computed at $P_u^{min} = 2825$ N. The corresponding computations in Fig. 20(b) for $\sigma_f = 0.3$ are found to be $\overline{P_u} = 3526$ N, COV = 0.098 and P_u^{min} =2712 N. For both cases, the computed lowest buckling loads correspond to an almost 50% reduction with respect to the buckling load of the perfect cylinder.

From the comparison of Figs. 20(a) and (b) with Figs. 15b and 16(b), which present the corresponding results obtained from the analysis of Combination 1 (geometric out-of-plane imperfections and geometric edge imperfections), a significant decrease of ~20% is observed in the predicted mean value, followed by a dramatic increase of more than 100% in the coefficient of variation, when all four sources of imperfections are simultaneously considered. Fig. 21 presents the experimental results reported in Arbocz and Abramovich (1979) for

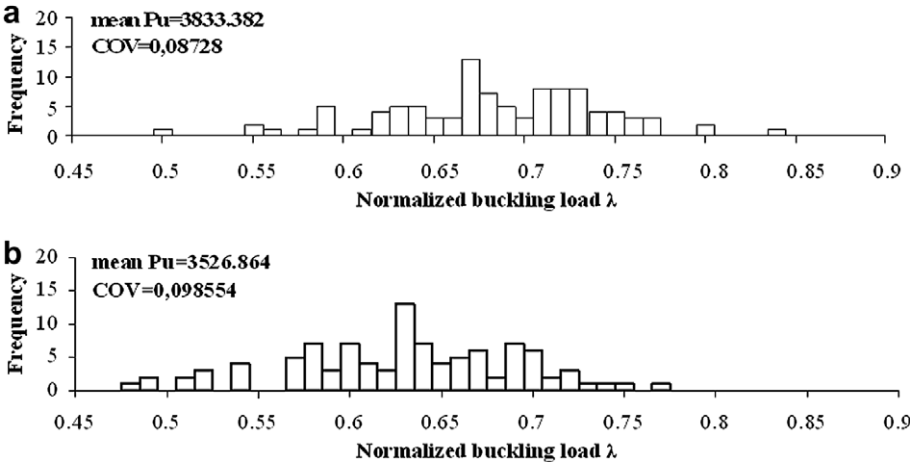

Fig. 20. Combination 3: Histogram of critical load factors for standard deviations of the applied axial loading (a) $\sigma_f = 0.2$ and (b) $\sigma_f = 0.3$.

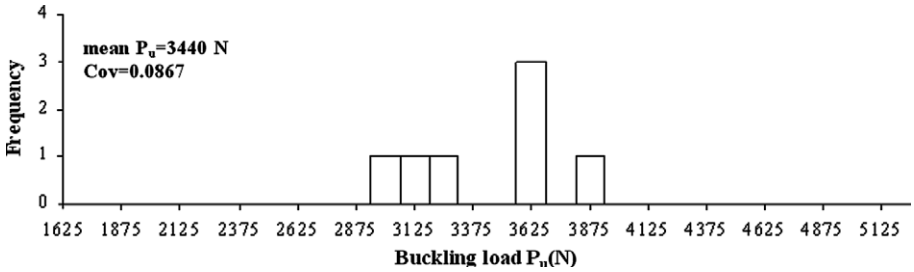

Fig. 21. Experimental results from 7 specimens in Koiter (1963).

7 specimens. The mean value of the measured experimental buckling loads is $\overline{P_u} = 3440$ N and the coefficient of variation is 0.0867. From the comparison of Figs. 20(a) and (b) and 21 it can be observed that using the proposed approach very close estimates of the scatter of the buckling load are obtained with respect to the experimental measurements. The predicted mean values and coefficient of variations of the buckling loads are very close to the corresponding ones determined experimentally. Finally, it is very interesting to observe the similarities in the unimodal shape of the predicted buckling load distribution and the corresponding shape of the experimental measurements. This observation proves further the validity of the proposed methodology in the sense that in addition to the 'worst case' studies, appropriate selection of parameters can also lead to a sufficiently close representation of experimental measurements.

6. Conclusions

In the present paper a simple and realistic approach is proposed for modeling the edge imperfections in the context of a sensitivity analysis, by assuming that these are produced by a non-uniform random axial load distribution. Thus, an edge deformation pattern is obtained at the very beginning of an incremental non-linear analysis procedure, which is assumed to correspond to the actual edge imperfections' pattern. Several arguments are provided in support of the aforementioned assumption. A one-dimensional homogeneous stochastic field is used for modeling the applied axial load. This varying axial load together with the initial (out-of-plane) geometric imperfections, thickness and material properties variability are incorporated in a cost-effective non-linear SFEM analysis using the non-linear TRIC shell element, while the variability of the limit loads is obtained by means of a brute-force Monte Carlo Simulation procedure. The numerical tests performed, highlighted the significant role of the non-uniform axial loading (or equivalently the uncertain boundary conditions) on the buckling behaviour of imperfection sensitive structures, like the thin-walled cylinder examined. Furthermore, reasonably closed estimates of the first and second order moments of the computed buckling loads as well as of the shape of its probability distribution with respect to experimental results were obtained for certain selected parameters, thus enhancing the validity of the proposed methodology.

References

Arbocz, J., 2000. The effect of imperfect boundary conditions on the collapse behaviour of anisotropic shells. Int. J. Solids Struct. 37, 6891–6915.

Arbocz, J., Abramovich, H., 1979. The initial imperfection data bank at the Delft University of Technology Part 1, Technical Report LR-290, Delft University of Technology, Department of Aerospace Engineering.

Arbocz, J., Babcock Jr., C.D., 1969. The effect of general imperfections on the buckling of cylindrical shells. J. Appl. Mech. 36 (1), 28–38.

Arbocz, J., Hol, J.M.A.M., 1991. Koiter's stability theory in a computer aided engineering (CAE) environment. Int. J. Solids Struct. 26 (9–10), 945–973.

Arbocz, J., Starnes Jr., J.H., 2002. Future directions and challenges in shell stability analysis. Thin Walled Struct. 40, 729–754.

Argyris, J.H., Tenek, L., Olofsson, L., 1997. *TRIC*, a simple but sophisticated 3 node triangular element based on 6 rigid-body and 12 straining modes for fast computational simulations of arbitrary isotropic and laminated composite shells. Comput. Methods Appl. Mech. Eng. 145, 11–85.

Argyris, J.H., Tenek, L., Papadrakakis, M., Apostolopoulou, D., 1998. Postbuckling performance of the TRIC natural mode triangular element for isotropic and laminated composite shells. Comput. Methods Appl. Mech. Eng. 166, 211–231.

Argyris, J.H., Papadrakakis, M., Stefanou, G., 2002. Stochastic finite element analysis of shells. Comput. Methods Appl. Mech. Eng. 191 (41–42), 4781–4804.

Elishakoff, I., 1985. Reliability approach to the random imperfection sensitivity of columns. Acta Mech. 55, 151–170.

Elishakoff, I., 2000. Uncertain buckling: its past, present and future. Int. J. Solids Struct. 37, 6869–6889.

Elishakoff, I., Arbocz, J., 1985. Reliability of axially compressed cylindrical shells with general non-symmetric imperfections. J. Appl. Mech. 52, 122–128.

Elishakoff, I., Li, Y.W., Starnes Jr., J.H., 2001. Nonclassical Problems in the Theory of Elastic Stability. Cambridge University Press, Cambridge, XVI, p. 336.

Greenberg, J.B., Stavsky, Y., 1995. Buckling of composite orthotropic cylindrical shells under non-uniform axial loads. Compos. Struct. 30, 399–406.

Hoff, N.J., Soong, T.C., 1969. Buckling of axially compressed circular shells with non-uniform boundary conditions. In: Proc. Symposium on Thin-walled Structures- their Design and Use in Building, University College of Swansea, pp. 61–80.

Koiter, W.T., 1963. The effect of axisymmetric imperfections on the buckling of cylindrical shells under axial compression. Prc Koninkl. Nederl Akademie van Wetenschappen 66 (B), 265–279.

Lagaros, N., Papadopoulos, V., 2006. Optimum design of shell structures with random geometric, material and thickness imperfections. Int. J. Solids Struct. 43 (22–23), 6948–6964.

Li, L.Y., 1990. Influence of loading imperfections on the stability of an axial compressed cylindrical shell. Thin Walled Struct. 10, 215–220.

Libai, A., Durban, D., 1977. Buckling of cylindrical shells subjected to non-uniform axial loads. ASME paper WA/APM-12.

Li, Y.W., Elishakoff, I., Starnes Jr., J.H., Bushnell, D., 1997. Effect of the thickness variation and initial imperfection on buckling of composite shells: asymptotic analysis and numerical results by BOSOR4 and PANDA2. Int. J. Solids Struct. 34, 3755–3767.

Lin, J., Zhao, Y., Zhang, Y., 2001. Accurate and highly efficient algorithms for structural stationary/non-stationary random responses. Comput. Methods Appl. Mech. Eng. 191 (1–2), 103–111.

Palassopoulos, G.V., 1977. Buckling analysis and design of imperfection sensitive structures. In: Haldar, A., Guran, A., Ayyub, B.M. (Eds.), Uncertainty Modeling in Finite Element, Fatigue and Stability of Systems, . In: Series on Stability, Vibration and Control of System Series B, vol. 9. World Scientific Publishing Company, Singapore, pp. 311–356.

Papadopoulos, V., Papadrakakis, M., 2004. Finite element analysis of cylindrical panels with random initial imperfections. J. Eng. Mech. ASCE 130 (8), 867–876.

Papadopoulos, V., Papadrakakis, M., 2005. The effect of material and thickness imperfections on the buckling load of shells with random initial imperfections. Comput. Methods Appl. Mech. Eng. 194 (12–16), 1405–1426.

Schenk, C.A., Schueller, G.I., 2003. Buckling analysis of cylindrical shells with random geometric imperfections. Int. J. Non-Linear Mech. 38, 1119–1132.

Schenk, C.A., Schueller, G.I., 2005. Uncertainty assessment of large finite element systems. In: Pfeiffer, F., Wriggers, P. (Eds.), Lecture Notes in Applied and Computational Mechanics. Springer, p. 24.

Shinozuka, M., Deodatis, G., 1996. Simulation of multi-dimensional Gaussian stochastic fields by spectral representation. Appl. Mech. Rev. ASME 49, 29–53.